International Journal of Automation and Computing 17(3), June 2020, 378-389
DOI: 10.1007/s11633-019-1195-6

Research on End-force Output of 8-cable Driven Parallel Manipulator

Sen-Hao Hou[1] Xiao-Qiang Tang[1,2] Ling Cao[1] Zhi-Wei Cui[1]
Hai-Ning Sun[1] Ying-Wei Yan[3]

[1]State Key Laboratory of Tribology, Department of Mechanical Engineering, Tsinghua University, Beijing 100084, China
[2]Beijing Key Lab of Precision/Ultra-precision Manufacturing Equipments and Control, Tsinghua University, Beijing 100084, China
[3]Postal Scientific Research and Planning Academy, Beijing 100096, China

Abstract: The return capsule needs to be launched to the moon and return back to earth in the third stage of the Chinese lunar exploration project. Therefore, it is necessary to perform simulations on the ground. This paper presents an 8-cable-driven parallel manipulator to achieve end-force output in a low-gravity environment. End-force output refers to the vector sum of the external force on the end-effector. A model of end-force output is established based on a kinematics model, a dynamic model, and a force analysis of an 8-cable driven parallel manipulator. To obtain end-force output in a low-gravity environment, the cable force has to be controlled to counteract gravity. In addition, a force-position mix control strategy is proposed to proactively control the cable force according to the force optimal distribution given by the closed-form force distribution method. Furthermore, a suitable choice for an end-force output is obtained by modeling the effect of cable force on end-force output. Experimental results show that the actual cable force agrees well with the calculated force distribution, indicating that it is feasible to realize end-force output in a low gravity environment.

Keywords: Cable driven parallel manipulators, low gravity environment, end-force output, cable force control, mix control strategy.

1 Introduction

Landing on the moon, building lunar bases, and exploring lunar resources have attracted increasing interest in space activities. In order to achieve this, it is important to launch the return capsule to the moon and ensure that it returns back to earth. The gravity on the moon is $\frac{1}{6}$ of that on earth. Besides, the sustainer thrust and pose of the rocket will have a high degree of coupling owing to the complex topography and soft soil on the lunar surface without fixed support. For a successful rocket launch from the moon, a great amount of analysis, calculation, and simulation need to be carried out on earth, which involves low-gravity simulations and launching the return capsule in any given direction. The launch of the return capsule can be regarded as end-force output, which is the vector sum of the external force on the end-effector, including cable force, gravity, and other forces acting on the end-effector.

Available technologies such as plane parabola, water tank, rigid parallel manipulator, single cable suspension mechanism and real object launch can realize simulations in a low-gravity environment. A novel dynamical model of parabolic flight was established by Karmal and Shelhamer[1]. This method can create a low gravity environment for a short time. However, due to the limited space in the aircraft, it is only suitable for astronaut training and scientific research. The buoyancy balance method[2] can counteract partial gravity by means of buoyancy of liquid in water tank, but the requirements of high-speed motion cannot be satisfied in the process of simulating launching the return capsule. The rigid parallel manipulator[3, 4] can achieve a small workspace in which the force is limited. A single cable suspension mechanism[5, 6] can counterbalance the force of gravity in a large workspace but confines the degree-of-freedom of motion. The technology of end-force output is not available in a non-vertical direction. Because of the high costs of real object launch, it is not a feasible way to achieve repetitive experiments. The realization of end-force output will be of considerable significance in the field of cable force control. Based on the single cable suspension mechanism, this study presents an 8-cable-driven parallel manipulator which can achieve end-force output in any direction in a low gravity environment.

Cable-driven parallel manipulators (CDPMs), which use flexible cables instead of rigid connectors, can achieve six degree-of-freedom motion. In the 1980s, scientists began to research CDPMs. Verhoeven[7] presented the relationship between the number of cables m and n de-

Research Article
Manuscript received March 7, 2019; accepted July 16, 2019; published online September 25, 2019
Recommended by Associate Editor Nazim Mir-Nasiri

grees of freedom. The system is defined by incompletely restrained positioning mechanisms (IRPMs) ($m < n + 1$), completely restrained positioning mechanisms (CRPMs) ($m = n + 1$), and redundantly restrained positioning mechanisms (RRPMs) ($m > n + 1$). In recent years, research on CDPMs has achieved rapid development. The technology has been applied to various fields[8–16], such as suspension, assembly, large radio telescope, macro gravity simulation, search-and-rescue operations in earthquakes, vehicle simulations, and gait training. The applications of the CDPMs mainly focus on the position control, in which the cable is required to be pulled and not broken. However, few applications of CDPMs are applied to end-force output. Compared with other equipment, the advantages of using the CDPMs are large workspace, low cost, high-speed motion and end-force output in any direction.

In the force distribution optimization design, Hiller et al.[17] presented the method of force distribution optimization in any RRPM system and proved the continuity of cable force in some trajectory. Mikelsons et al.[18] improved the above method. They presented a fast solution method and time-optimal trajectories on the basis of continuity, which can be applied to a real-time system. Tang et al.[19] discussed the relation between cable tension and workspace. Gosselin and Grenier[20] adopted the p-norms cable force distribution method. Pott et al.[21] presented a closed-form method to calculate the cable force distribution, which greatly improved the calculation efficiency. Compared with the existing cable force distribution methods, the closed-form method is more suitable for an 8-cable-driven parallel manipulator due to its high efficiency. In addition, scholars presented different optimization algorithms[22–24] considering parameters such as minimum power and mean force. Lamine et al.[25] presented a method to design CDPMs by using interval analysis. Zhang et al.[26] designed a position/force hybrid control system for a gripper. Zhang et al.[27] analyzed the motion-force transmissibility characteristics based on the parallel machine. Mostly, the methods are applied to numerical simulation and other mechanisms. Few studies have focused on controlling the cable force and analysing the results of force optimization based on the CDPMs.

In this study, we use the 8-cable-driven parallel manipulator shown in Fig. 1 to simulate the low-gravity environment and achieve end-force output in such an environment. A model based on end-force output is established. Then, a force–position mix control strategy is proposed to control the cable force according to the force optimal distribution. The results of the cable force control and end-force output are verified by the experiment.

This paper is organized as follows. Section 2 presents the kinematic and dynamic modelling of the 8-cable-driven parallel manipulator is established. In Section 3, the processes of end-force output and the force distribution method are described. Then, Section 4 presents the simulations performed in a low-gravity environment and experiments of end-force output are performed, and the results are presented in Section 5. Finally, Section 6 presents the conclusions of this study and discusses ongoing work.

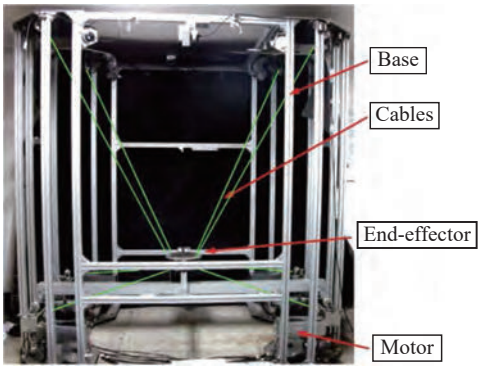

Fig. 1 Eight-cable driven parallel manipulator

2 Modeling

The 8-cable-driven parallel manipulator considered in this study is shown in Fig. 1. Eight cables are connected in parallel to the end-effector of motors mounted on a fixed base and control the end-effector by exerting tensions on the cables. Four connections are located in the upper part of the end-effector and the other four connections are located at the bottom. The motors mounted at the bottom of the fixed base are connected to the upper four cables through pulleys. The kinematic architecture and force system of the 8-cable-driven parallel manipulator is shown in Fig. 2.

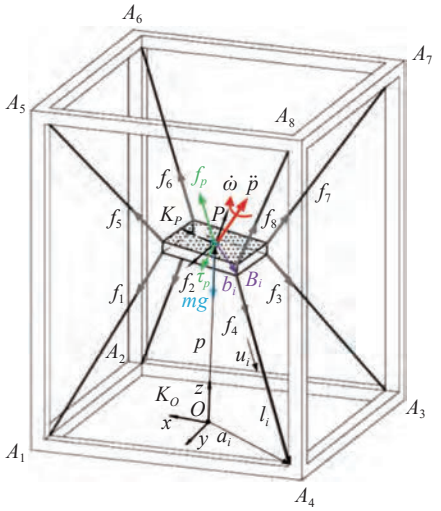

Fig. 2 Kinematic architecture and force system of 8-cable-driven parallel manipulator

In Fig. 2, K_O is the base frame that is defined with its origin at the middle point O of the bottom surface of the fixed base. The frame K_P is fixed at a middle point P of the upper surface of the end-effector. The position of the end-effector can be given as $\boldsymbol{p} = [x_P \; y_P \; z_P]^{\mathrm{T}}$ in frame

K_O. The orientation of the end-effector can be described by a space-three rotation sequence of α about the x-axis, β about the y-axis, and γ about the z-axis. The six variables of the pose of the end-effector are denoted by $\boldsymbol{X} = [x_P \quad y_P \quad z_P \quad \alpha \quad \beta \quad \gamma]^{\mathrm{T}}$.

It is assumed that the cables are straight without considering the cable sagging effect because the span of cables are limited. $A_i\,(i = 1, 2, \cdots, 8)$ and $B_i\,(i = 1, 2, \cdots, 8)$ are the two attaching points of the eight cables on the base and end-effector, respectively. The positions of the two attaching points are represented by vectors $\boldsymbol{a}_i$ and ${}^P\boldsymbol{b}_i$, where $\boldsymbol{a}_i\,(i = 1, 2, \cdots, 8)$ and ${}^P\boldsymbol{b}_i\,(i = 1, 2, \cdots, 8)$ are constant vectors in the base frame K_O and end-effector frame K_P, respectively. $\boldsymbol{l}_i\,(i = 1, 2, \cdots, 8)$ is the vector along the cable and has the same length as the cable. Under kinematics modeling, the position of the end-effector can be denoted as

$$l_i = a_i - p - \boldsymbol{R} \cdot {}^P b_i, \qquad (i = 1, 2, \cdots, 8)\,. \tag{1}$$

The unit vector along the cable can be denoted as

$$\boldsymbol{u}_i = \frac{\boldsymbol{l}_i}{|\boldsymbol{l}_i|} = \frac{\boldsymbol{a}_i - \boldsymbol{p} - \boldsymbol{R} \cdot {}^P\boldsymbol{b}_i}{|\boldsymbol{a}_i - \boldsymbol{p} - \boldsymbol{R} \cdot {}^P\boldsymbol{b}_i|}, \qquad (i = 1, 2, \cdots, 8) \tag{2}$$

where $\boldsymbol{R}$ is the rotation matrix of the end-effector frame K_P relative to the base frame K_O, which can be denoted as

$$\boldsymbol{R} = \boldsymbol{R}(z, \gamma)\,\boldsymbol{R}(y, \beta)\,\boldsymbol{R}(x, \alpha) = \begin{bmatrix} c\gamma c\beta & c\gamma s\beta s\alpha - s\gamma c\alpha & c\gamma s\beta c\alpha + s\gamma s\alpha \\ s\gamma c\beta & s\gamma s\beta s\alpha - c\gamma c\alpha & s\gamma s\beta c\alpha - c\gamma s\alpha \\ -s\beta & c\beta s\alpha & c\beta c\alpha \end{bmatrix}.$$

From (1),

$$\begin{aligned} \boldsymbol{l}_i^2 &= [\boldsymbol{a}_i - \boldsymbol{p} - \boldsymbol{b}_i]^{\mathrm{T}}\,[\boldsymbol{a}_i - \boldsymbol{p} - \boldsymbol{b}_i] \\ \boldsymbol{b}_i &= \boldsymbol{R} \cdot {}^P\boldsymbol{b}_i. \end{aligned} \tag{3}$$

Differentiating (3) with respect to time, and then organizing the equations into matrix form, we obtain

$$\dot{\boldsymbol{l}} = -\boldsymbol{A}\dot{\boldsymbol{X}} \tag{4}$$

$$\dot{\boldsymbol{l}} = [\dot{l}_1 \quad \dot{l}_2 \quad \cdots \quad \dot{l}_8]^{\mathrm{T}}$$

$$\boldsymbol{A}^{\mathrm{T}} = \begin{bmatrix} \boldsymbol{u}_1 & \cdots & \boldsymbol{u}_8 \\ \boldsymbol{b}_1 \times \boldsymbol{u}_1 & \cdots & \boldsymbol{b}_8 \times \boldsymbol{u}_8 \end{bmatrix}$$

$$\dot{\boldsymbol{X}} = \begin{bmatrix} \dot{\boldsymbol{p}} \\ \boldsymbol{\omega} \end{bmatrix} = [\dot{x}_P \quad \dot{y}_P \quad \dot{z}_P \quad \omega_x \quad \omega_y \quad \omega_z]^{\mathrm{T}}.$$

In the above equations, vector $\dot{\boldsymbol{p}}$ represents the linear velocity of point P and vector $\boldsymbol{\omega}$ denotes the angular velocity of the end-effector. For the 8-cable-driven parallel manipulator considered in this study, the mass of the cables can be negligible compared with those of the end-effector and payload. In other words, each cable can be modeled as a massless string, which will simplify the dynamic modelling of this cable-driven robot. Under this assumption, the dynamic model of this cable-driven robot with respect to point P is obtained using the Newton-Euler method as follows:

$$\boldsymbol{A}^{\mathrm{T}}\boldsymbol{f} + \boldsymbol{\omega}_{\mathrm{P}} + \boldsymbol{\omega}_g = \boldsymbol{M}\ddot{\boldsymbol{X}} + \boldsymbol{N}\dot{\boldsymbol{X}} \tag{5}$$

which can be simplified to

$$\boldsymbol{A}^{\mathrm{T}}\boldsymbol{f} + \boldsymbol{\omega} = 0 \tag{6}$$

$$\boldsymbol{f} = [f_1 \quad f_2 \quad \cdots \quad f_8]^{\mathrm{T}}, \quad f_i > 0 \quad (i = 1, 2, \cdots, 8)$$

$$\boldsymbol{\omega} = \boldsymbol{\omega}_P + \boldsymbol{\omega}_g - \boldsymbol{M}\ddot{\boldsymbol{X}} - \boldsymbol{N}\dot{\boldsymbol{X}}$$

$$\ddot{\boldsymbol{X}} = \begin{bmatrix} \ddot{\boldsymbol{p}} \\ \dot{\boldsymbol{\omega}} \end{bmatrix} = [\ddot{x}_P \quad \ddot{y}_P \quad \ddot{z}_P \quad \dot{\omega}_x \quad \dot{\omega}_y \quad \dot{\omega}_z]^{\mathrm{T}}$$

$$\boldsymbol{M} = \begin{bmatrix} m\boldsymbol{I} & -m\boldsymbol{c}^{\times} \\ m\boldsymbol{c}^{\times} & \boldsymbol{I} \end{bmatrix}, \ \boldsymbol{N} = \begin{bmatrix} \boldsymbol{0} & -m(\boldsymbol{\omega} \times \boldsymbol{c})^{\times} \\ m(\boldsymbol{\omega} \times \boldsymbol{c})^{\times} & -(\boldsymbol{I}\boldsymbol{\omega})^{\times} \end{bmatrix}$$

$$\boldsymbol{\omega}_P = \begin{bmatrix} \boldsymbol{f}_P \\ \boldsymbol{\tau}_P \end{bmatrix}, \ \boldsymbol{\omega}_g = \begin{bmatrix} m\boldsymbol{g} \\ \boldsymbol{c} \times m\boldsymbol{g} \end{bmatrix}.$$

In the above equations, vector $\ddot{p}$ represents the linear acceleration of point P and vector $\dot{\boldsymbol{\omega}}$ denotes the angular acceleration of the end-effector. $\boldsymbol{f}$ is a vector consisting of eight individual cable forces. The individual cable force can be denoted as $\boldsymbol{f}_i = f_i\boldsymbol{u}_i = \dfrac{f_i\boldsymbol{l}_i}{\|\boldsymbol{l}_i\|}, (i = 1, 2, \cdots, 8)$. $\boldsymbol{f}_P$ and $\boldsymbol{\tau}_P$ are the external force and moment applied to point P. m is the mass of the end-effector and load, and $\boldsymbol{g}$ is the acceleration due to gravity. $\boldsymbol{I}$ is the moment of the end-effector and load about its center of mess with respect to the basic vectors of frame K_O. $\boldsymbol{c}$ is the position vector of the center of mass of the end-effector in frame K_P. $(\,)^{\times}$ is an operator, representing the transformation from vector to matrix form.

From dynamic (6), one can find a set of cable forces at any given motion conditions. Because a cable has to maintain tension ($f_i > 0$), the solution of (6) will not always be feasible. Moreover, the 8-cable-driven parallel manipulators are redundantly actuated so that (6) is indeterminate. In other words, (6) will have multiple solutions. Therefore, a force optimal distribution is required, which will be addressed in the next section.

3 End-force output and force distribution in low gravity environment

3.1 End-force output in low-gravity environment

The end-force output is to produce a specified force by

the end-effector along the designated direction, which has to remain parallel to the normal direction of end-effector, by controlling the cable force. Meanwhile, the end-effector will be driven in accelerated motion because of the combined forces of cables and gravity. To simulate the low-gravity environment and obtain the end-force output in such an environment, the cable force should be controlled to drive the accelerated motion of the end-effector and counteract gravity simultaneously. As shown in Fig. 3, the combined force $\boldsymbol{f}$ of the 8-cable-driven force can be defined into two parts as follows:

$$\boldsymbol{f} = \boldsymbol{f}_g + \boldsymbol{f}_m \tag{7}$$

$$\boldsymbol{F} = \boldsymbol{G} + \boldsymbol{f} = m\boldsymbol{a} \tag{8}$$

$$\boldsymbol{F} = \boldsymbol{G}^{'} + \boldsymbol{f}_m = m\boldsymbol{a} \tag{9}$$

$$\boldsymbol{G}^{'} = \alpha m\boldsymbol{g},\ \boldsymbol{G} = m\boldsymbol{g},\ \boldsymbol{f}_g = -(1-\alpha)m\boldsymbol{g}. \tag{10}$$

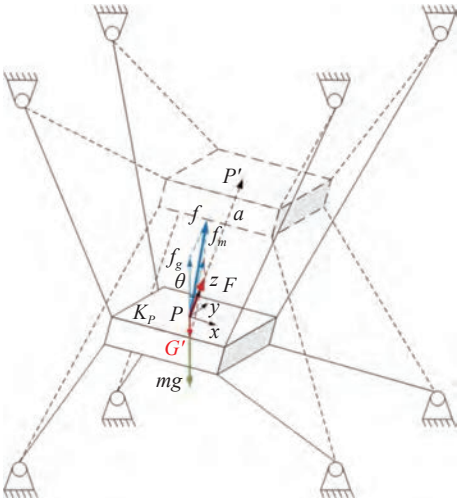

Fig. 3 End-force output

In the above equations, $\boldsymbol{f}_g$ is one component of $\boldsymbol{f}$ used for counteracting part of gravity to simulate a low-gravity environment. $\boldsymbol{G}^{'} = \alpha m\boldsymbol{g}$ is the gravity of the end-effector and load in a low-gravity environment. $\boldsymbol{f}_m$ is another component to drive the motion of the end-effector in low gravity. $\boldsymbol{F}$ denotes the combined force of $\boldsymbol{G}$ and $\boldsymbol{f}$. It is also considered to be the combined force of $\boldsymbol{G}^{'}$ and $\boldsymbol{f}_m$ in a low-gravity environment, which is the end-force output of the end-effector according to experimental requirement. Let the position of point P in frame K_O be given by $[x_P,\ y_P,\ z_P]^{\mathrm{T}}$. The acceleration of point P is then given by $\boldsymbol{a} = [\ddot{x}_P,\ \ddot{y}_P,\ \ddot{z}_P]^{\mathrm{T}}$. Further, the end-effector is driven to move in acceleration $\boldsymbol{a}$ due to the force $\boldsymbol{F}$.

In the movement of the end-force output, the direction of the combined force $\boldsymbol{F}$ is similar to that of velocity and acceleration of the end-effector because the direction of the end-force output has to remain parallel to the normal direction of the end-effector, which implies that the end-effector has to maintain a fixed orientation. Thus, ideally, the angular velocity should be $\boldsymbol{\omega} = \boldsymbol{0}$, and the angular acceleration should be $\dot{\boldsymbol{\omega}} = \boldsymbol{0}$.

For the 8-cable-driven parallel manipulator considered in this study, weights are used for the loads mounted on the end-effector. It is assumed that the center gravity of the end-effector and load overlaps at point P, i.e., $\boldsymbol{c} = \boldsymbol{0}$, because the size of the end-effector is limited. The Coriolis force, which is denoted by $\boldsymbol{N}$ in the dynamic (6), can be ignored in the movement of the end-force output. Besides, there are no external forces and torques acting on the end-effector. Therefore, the dynamic (6) can be simplified to

$$\begin{bmatrix} \boldsymbol{u}_1 & \cdots & \boldsymbol{u}_8 \\ \boldsymbol{b}_1 \times \boldsymbol{u}_1 & \cdots & \boldsymbol{b}_8 \times \boldsymbol{u}_8 \end{bmatrix} \begin{bmatrix} \boldsymbol{f}_1 \\ \vdots \\ \boldsymbol{f}_8 \end{bmatrix} + \boldsymbol{M} \begin{bmatrix} \boldsymbol{g} - \boldsymbol{a} \\ \boldsymbol{0} \end{bmatrix} = \boldsymbol{0}. \tag{11}$$

By substituting (11) into (9) and (10), we obtain

$$\begin{bmatrix} \boldsymbol{u}_1 & \cdots & \boldsymbol{u}_8 \\ \boldsymbol{b}_1 \times \boldsymbol{u}_1 & \cdots & \boldsymbol{b}_8 \times \boldsymbol{u}_8 \end{bmatrix} \begin{bmatrix} \boldsymbol{f}_{g1} \\ \vdots \\ \boldsymbol{f}_{g8} \end{bmatrix} + \boldsymbol{M} \begin{bmatrix} (1-\alpha)\,\boldsymbol{g} \\ \boldsymbol{0} \end{bmatrix} = \boldsymbol{0} \tag{12}$$

$$\begin{bmatrix} \boldsymbol{u}_1 & \cdots & \boldsymbol{u}_8 \\ \boldsymbol{b}_1 \times \boldsymbol{u}_1 & \cdots & \boldsymbol{b}_8 \times \boldsymbol{u}_8 \end{bmatrix} \begin{bmatrix} \boldsymbol{f}_{m1} \\ \vdots \\ \boldsymbol{f}_{m8} \end{bmatrix} + \boldsymbol{M} \begin{bmatrix} \alpha\boldsymbol{g} - \boldsymbol{a} \\ \boldsymbol{0} \end{bmatrix} = \boldsymbol{0}. \tag{13}$$

From (12) and (13), one has the components $\boldsymbol{f}_g$, $\boldsymbol{f}_m$. The force of the eight cables $\boldsymbol{f}$ can be computed from (7).

For the simulation of the end-force output in a low-gravity environment, controlling the cable force is one of the most important process, which requires an optimal cable force distribution. The method of cable force distribution will be addressed in the next section.

3.2 Method of cable force distribution

For the 8-cable-driven parallel manipulator considered in this study, the cable force distribution is to compute the solutions of (12), (13) which is satisfied by the requirements of the force control. The solution should be in the feasible region given by the bounds $f_{\min}$, $f_{\max}$ to avoid cable over-sagging and overload of the motors. The basic problem of force distribution can be written as follows:

$$\boldsymbol{A}^{\mathrm{T}}\boldsymbol{f} + \boldsymbol{\omega} = \boldsymbol{0},\ (f_1, \cdots, f_8) \in [f_{\min}, f_{\max}]\,. \tag{14}$$

Moreover, the 8-cable-driven parallel manipulator is designed for end-force output. Therefore, the force distribution has to be continuous along the trajectory of the end-effector to satisfy the real-time control requirement

and reduce vibration.

The cable force distribution satisfying the above requirements can be given by the closed-form force distribution method presented by Pott et al.[21]. The problem of force distribution (14) can be converted to a solution of two-norm optimization as follows:

$$\begin{aligned} &\min \|\boldsymbol{f}_v\|_2 = \min \|\boldsymbol{f} - \boldsymbol{f}_m\|_2 \\ &\text{s.t.} \begin{cases} \boldsymbol{A}^{\mathrm{T}} \boldsymbol{f}_v = -\boldsymbol{\omega} - \boldsymbol{A}^{\mathrm{T}} \boldsymbol{f}_m \\ f_{\min} \le f_i \le f_{\max}, i = 1, 2, \cdots, 8 \end{cases} \end{aligned} \tag{15}$$

where $\boldsymbol{f} = \boldsymbol{f}_m + \boldsymbol{f}_v$, $f_{m,i} = \dfrac{f_{\min} + f_{\max}}{2}$, $(i = 1, 2, \cdots, 8)$. The result of (15) can be obtained using Moore-Penrose generalized inverse, yielding

$$\boldsymbol{f} = \boldsymbol{f}_m - \boldsymbol{A}^{+\mathrm{T}} \left(\boldsymbol{\omega} - \boldsymbol{A}^{\mathrm{T}} \boldsymbol{f}_m \right). \tag{16}$$

The resulting force distribution $\boldsymbol{f}$ is the final result if it is in the force range given by the bounds $f_{\min}$, $f_{\max}$.

The geometrical properties of the 8-cable-driven parallel manipulator are listed in Table 1. The mass of the end-effector is $m_e = 0.5\,\mathrm{kg}$, and the load is $m_l = 5\,\mathrm{kg}$. The force bounds are $f_{\min} = 10\,\mathrm{N}$, $f_{\max} = 100\,\mathrm{N}$. The 8-cable-driven parallel manipulator is used to output an end-force $\boldsymbol{F}$ in a $\dfrac{1}{20}$ gravity environment $\left(\alpha = \dfrac{1}{20}\right)$ along the trajectory shown in Fig. 3. The magnitude of the end-force is $F = ma = 5.5\,\mathrm{kg} \times 0.2\,\mathrm{m/s^2} = 1.1\,\mathrm{N}$, and the direction of $\boldsymbol{F}$ is $\beta = 5^\circ$ between the z-axis and vertical direction in the XPZ plane. The acceleration of the end-effector is $a = 0.2\,\mathrm{m/s^2}$. As shown in Fig. 4, the force distribution can be obtained using the closed-form force distribution method in this situation.

Table 1 Geometrical properties of the 8-cable-driven parallel manipulator

Cable i	End-effector vector ${}^P\boldsymbol{b}_i$ (m)	Base vector $\boldsymbol{a}_i$ (m)
1	(0.045, 0.045, 0)	(0.790, 0.520, 0)
2	(0.045, –0.045, 0)	(0.790, –0.520, 0)
3	(–0.045, –0.045, 0)	(–0.790, –0.520, 0)
4	(–0.045, 0.045, 0)	(–0.790, 0.520, 0)
5	(0.045, 0.045, –0.085)	(0.790, 0.520, 1.780)
7	(–0.045, –0.045, –0.085)	(–0.790, –0.520, 1.780)
8	(–0.045, 0.045, –0.085)	(–0.790, 0.520, 1.780)

4 Optimization of pre-tightening force for end-force output

4.1 Modeling of the effect of the cable force on end-force output

In practical cases of end-force output, the results of the end-force output will deviate from the ideal value under error control of cable force. As shown in Fig. 5, the cable forces differ from the ideal value so that the direction of composition of the cable forces f and gravity mg could not remain in the ideal direction, which is along the normal direction of the end-effector. Furthermore, the acceleration error of the end-effector will be influenced by

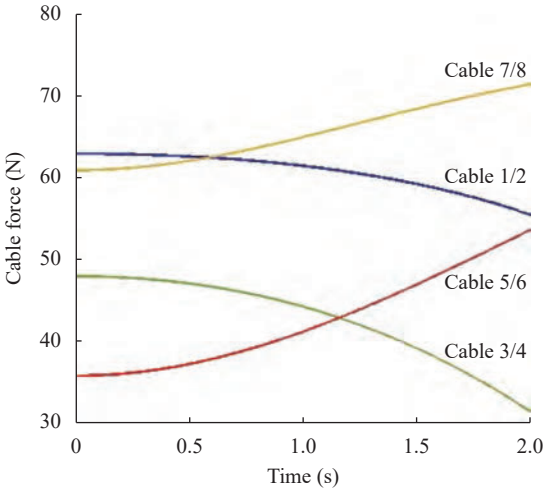

Fig. 4 Force distribution by closed-form force distribution method

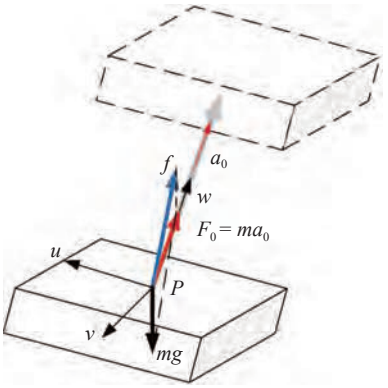

(a) Ideal situation

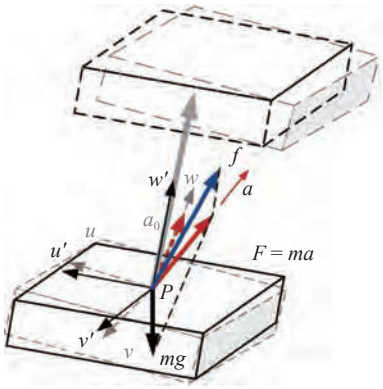

(b) Practical situation

Fig. 5 Situation of end-force output

the bias of composition force. We can choose the pose and acceleration value of the end-effector to describe the situation of end-force output in practical cases.

On using Newton-Euler's laws, the equations of the practical motion of the end-effector can be written in the following form:

$$\begin{cases} \boldsymbol{A}^{\mathrm{T}}(\boldsymbol{X})\boldsymbol{f} = \boldsymbol{M}\ddot{\boldsymbol{X}} = \begin{bmatrix} m\ddot{x}_P \\ m\ddot{y}_P \\ m\left(\ddot{z}_P + g\right) \\ \boldsymbol{I}\begin{bmatrix} \ddot{\alpha} \\ \ddot{\beta} \\ \ddot{\gamma} \end{bmatrix} \end{bmatrix} \\ \boldsymbol{X}_0 = \boldsymbol{X}^* \\ t \in (0, T) \end{cases} \tag{17}$$

where $\boldsymbol{X} = [x_P \;\; y_P \;\; z_P \;\; \alpha \;\; \beta \;\; \gamma]^{\mathrm{T}}$ is the practical pose of the end-effector. $\boldsymbol{f}$ is a vector consisting of eight practical values of cable forces. Equation (17) is a differential coefficient equation group involving $\boldsymbol{X}$. The initial value $\boldsymbol{X}_0$ of the end-effector in the movement of end-force output is given by $\boldsymbol{X}^* = [x_P^* \;\; y_P^* \;\; z_P^* \;\; \alpha^* \;\; \beta^* \;\; \gamma^*]^{\mathrm{T}}$. T is the total time of end-force output movement.

The numerical solution of equation (17) can be obtained by a discrete model in time. At any given time t_i in the process of end-force output, the practical pose of the end-effector can be given by $\boldsymbol{X}(t_i)$. The total time of movement T can be divided into small time intervals given by

$$\Delta t_i = [t_i, t_{i+1}], \quad i = 0, 1, \cdots, N-1. \tag{18}$$

For the time interval Δt_i, the practical pose of the end-effector at any moment $t \in [t_i, t_{i+1}]$ can be described as $\boldsymbol{X}^i(t)$. Therefore, in any time interval Δt_i, a differential coefficient equation group involving $\boldsymbol{X}$ can be described as

$$\begin{cases} \mathbf{A}^{\mathrm{T}}(\boldsymbol{X}(t))\boldsymbol{f}_i = \boldsymbol{M}\ddot{\boldsymbol{X}}(t) \\ \boldsymbol{X}_0^i = \boldsymbol{X}^{i-1}(t_i), \; (i = 1, 2, \cdots, N-1) \\ \boldsymbol{X}_0^i = \boldsymbol{X}^*, \; (i = 0) \\ t \in (t_i, t_{i+1}) \end{cases} \tag{19}$$

where $\boldsymbol{f}_i = \boldsymbol{f}_i(\boldsymbol{X}_i)$ is a vector, consisting of eight individual cable forces according to the pose of the end-effector at the given time interval Δt_i, which can be solved using the close-form cable force distribution method mentioned in Section 2. The cable forces $\boldsymbol{f}_i$ is constant during the time interval Δt_i. Let the initial value of the time interval Δt_i be given by $\boldsymbol{X}_0^i$. By obtaining a discrete solution to the differential coefficient equation given by (19), one can obtain the pose $\boldsymbol{X}^i(t_{i+1})$ of the end-effector at moment t_{i+1} in the time interval $\Delta t_i = [t_i, \; t_{i+1}]$, which can be used as the initial value of $\boldsymbol{X}_0^{i+1}$ in the time interval Δt_{i+1}. Therefore, the discrete solution $\bar{\boldsymbol{X}} = [\boldsymbol{X}(t_0), \boldsymbol{X}(t_1), \cdots, \boldsymbol{X}(t_N),]$ is obtained in the total time of movement T. If the time interval Δt_i is sufficiently small, $\bar{\boldsymbol{X}}$ could be regarded as the solution to the dynamics equation given in (17).

4.2 Optimization of pre-tightening force for end-force output

For the 8-cable-driven parallel mechanism considered in this study, the cable force distribution is a multi-solution problem. The pre-tightening force $\boldsymbol{F}_{pre}$ is defined as the minimum of each cable force distribution. The pre-tightening force $\boldsymbol{F}_{pre}$ differs under different results of cable force distribution. To obtain a good effect of end-force output, a major issue in real control is to choose a reasonable pre-tightening force $\boldsymbol{F}_{pre}$. The cable force distribution under different values of $\boldsymbol{F}_{pre}$ can be calculated using the closed-form force distribution method mentioned in Section 2 by adjusting the value of $\boldsymbol{f}_m$, which represents the boundary condition of the two-norm optimization problem given by (15).

In actual control, the practical cable force usually fluctuates according to the ideal cable force. The fluctuating error can be simplified into sine waveforms. Under the same fluctuating error, the cable force distributions for different values of $\boldsymbol{F}_{pre}$ are shown in Fig. 6. The total mass of the load and end-effector is $m = 5.5\,\mathrm{kg}$. The acceleration of the end-effector is $a = 0.2\,\mathrm{m/s^2}$. The attitude angle of the end-effector is (0°, 5°, 0°). The value of the end-force is $F = ma = 5.5\,\mathrm{kg} \times 0.2\,\mathrm{m/s^2} = 1.1\,\mathrm{N}$. The direction of $\boldsymbol{F}$ is along the normal direction of the surface of the end-effector. The calculation of cable force distribution is according to the ideal end-force output. In actual control, the practical cable forces will approach that ideal value.

Using the effect of cable force on end-force output addressed in Section 3.1, the practical value of acceleration a and pose $\boldsymbol{X}$ of the end-effector are shown in Fig. 7.

As shown in Fig. 7, the error in the value of acceleration a becomes larger with the increase in $\boldsymbol{F}_{pre}$, but the error in the attitude angle becomes smaller. Using the error index shown in (20), we can evaluate the error conditions of the practical value of acceleration a and attitude angle β for different values of $\boldsymbol{F}_{pre}$ shown in Fig. 8, which indicate the effect of end-force output. Let $\eta = 0.5$, the suitable value of $\boldsymbol{F}_{pre}$ is obtained as shown in Fig. 8.

$$\begin{aligned} \varepsilon &= \eta\varepsilon_{acc} + (1-\eta)\varepsilon_{angle,\beta} \\ \varepsilon_{acc} &= \frac{\max(\delta_a)}{|a_0|}, \; \varepsilon_{angle,\beta} = \frac{\max(\delta_\beta)}{\beta_0}. \end{aligned} \tag{20}$$

From Fig. 9, we know that the suitable value of $\boldsymbol{F}_{pre}$ for a total mass of 5 kg is $\boldsymbol{F}_{pre} = 15\,\mathrm{N}$. The value of $\boldsymbol{F}_{pre}$ varies under different loads. As the load increases, the

suitable value of $\boldsymbol{F}_{pre}$ becomes larger, which obtains a

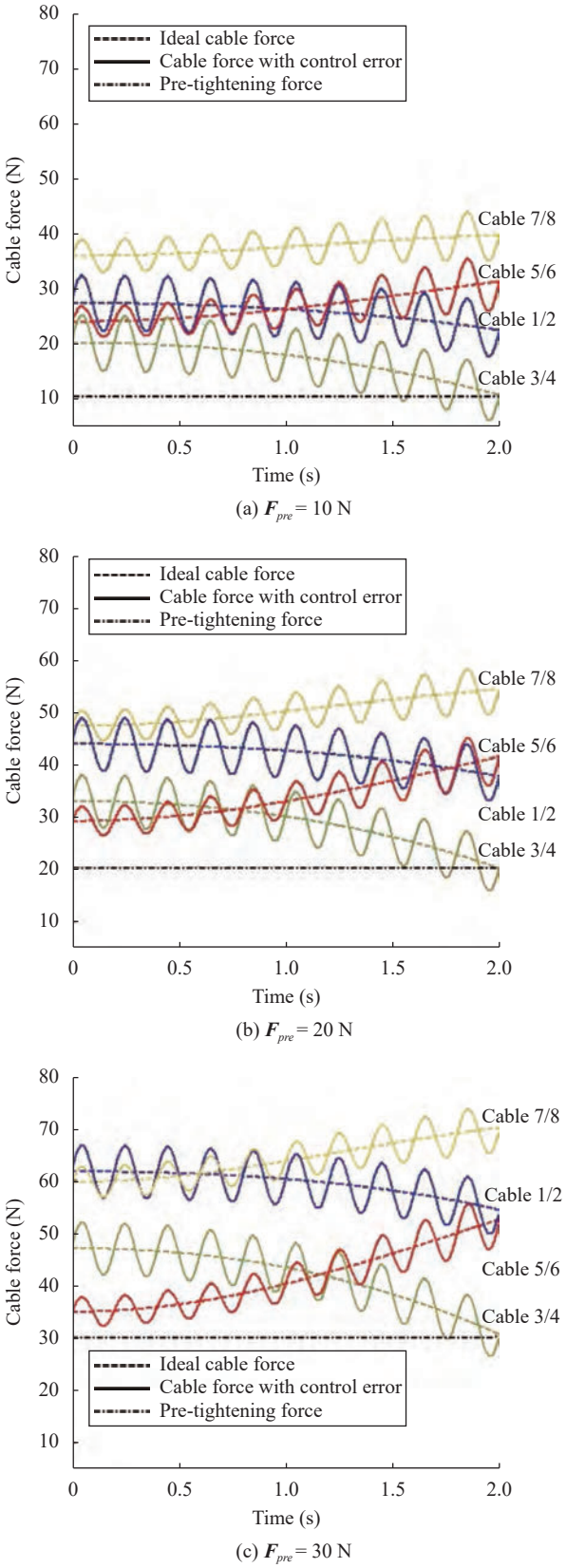

(a) $\boldsymbol{F}_{pre}$ = 10 N

(b) $\boldsymbol{F}_{pre}$ = 20 N

(c) $\boldsymbol{F}_{pre}$ = 30 N

Fig. 6 Cable force distributions in different $\boldsymbol{F}_{pre}$

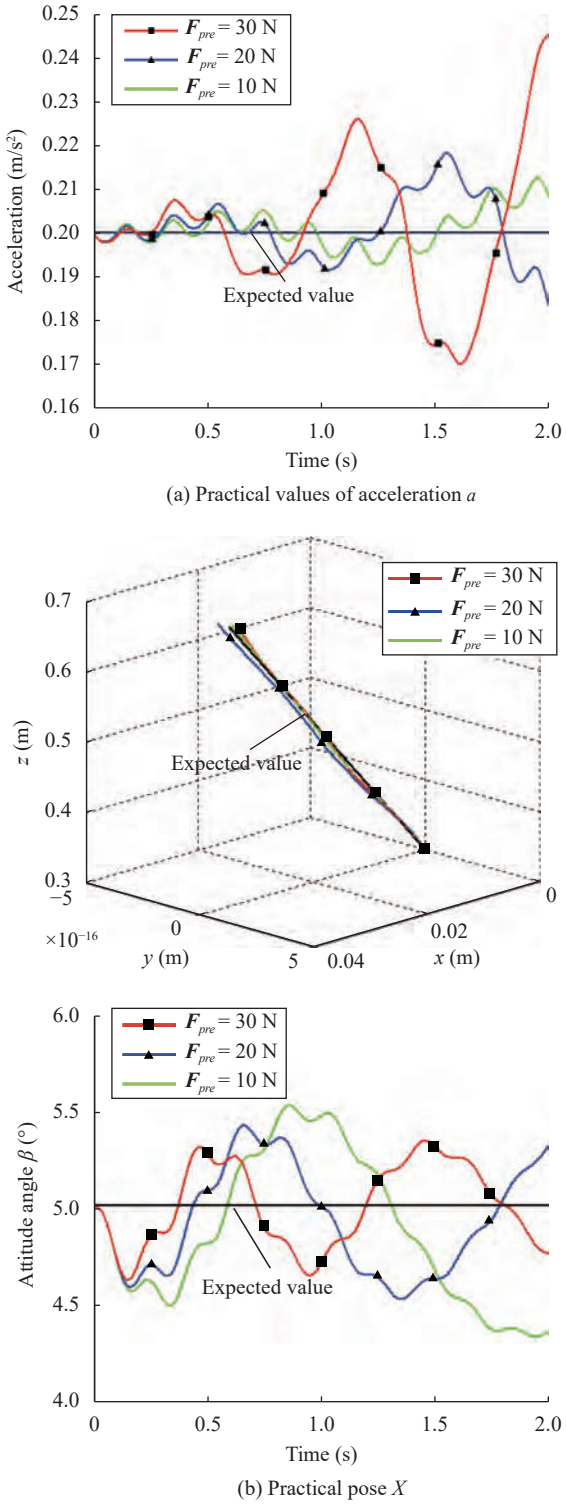

(a) Practical values of acceleration a

(b) Practical pose X

Fig. 7 Effect of end-force output for different values of $\boldsymbol{F}_{pre}$

better effect of end-force output.

5 Cable force control and experiment results

In the simulation experiment of end-force output in

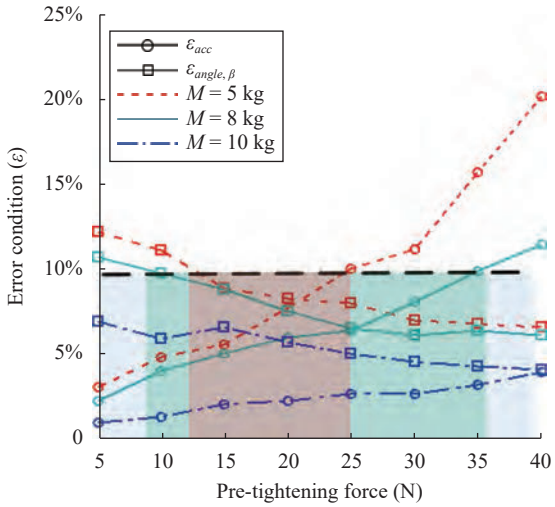

Fig. 8 Error conditions for different values of $\boldsymbol{F}_{pre}$

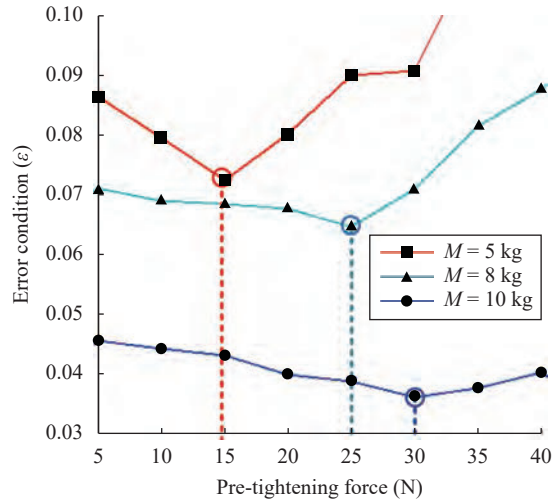

Fig. 9 Optimization of $\boldsymbol{F}_{pre}$

the low environment, the end-effector has to be driven in specified motion by cables. At the same time, each cable force $\boldsymbol{f}_i$ has to be controlled to counteract part of gravity and make the combined force $\boldsymbol{F}$ acting on the end-effector to satisfy the experiment design. In this paper, the 8-cable driven parallel manipulator mentioned above is applied to that simulation experiment.

5.1 Experiment equipment description and cable force control strategy

As shown in Fig. 10, the experimental system consists of an 8-cable-driven parallel manipulator, a control system, and a measuring system. The Turbo Programmable Multi-Axis Controller (PMAC) in the control system is used to control the motors under motion program. The measuring system consists of force sensors (DJSX-44-100 kg) and linear wire encoders, which are used for measuring the cable force and position of the end-effector, respectively. Based on the measuring feedback, each cable force $\boldsymbol{f}_i$ is controlled by the control system. The control frequency is 100 Hz, and the measuring frequency is 200 Hz.

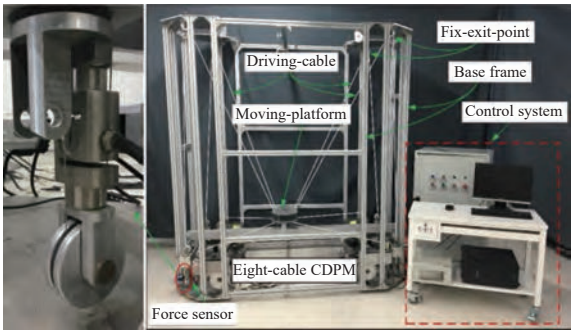

Fig. 10 Experiment system of 8-cable driven parallel manipulator

The force-position mix control strategy is applied to cable force control. As shown in the control strategy block in Fig. 11, the motors drive the variation of each cable length under the motion program by using the control system. Meanwhile, each cable length will be adjusted per control cycle by comparing results between the measuring force f and force distribution f_0. For example, the cable will be pulled in unit length based on the original length given by the motion program if $f_0 - f > 0$. Therefore, the force-position mix control strategy can control the motion of the end-effector and vary the cable force according to the results of force distribution simultaneously.

5.2 Simulation experiment of low gravity environment

First, the 8-cable-driven parallel manipulator is applied to simulate the low-gravity environment and achieve the specified motion in that environment. Because the end-force can be applied accurately by controlling the cable force, the end-effector can move in space with a given acceleration. For instance, when the end-effector moves with a horizontal projection motion, a low gravity environment is created because part of the gravity is counteracted by the component of the cable force. The experiment is designed to simulate an environment whose gravity is $\frac{1}{20}$ of that on earth. In that environment, the end-effector, which has a horizontal velocity, will move under the $\frac{1}{20}$ gravity with horizontal projection. The total mass of the end-effector and load is 5.5 kg. The horizontal velocity v_0 is 0.01 m/s. The end-effector has a –10° rotation about the y-axis. The motion state of the end-effector is shown in Fig. 12. The actual displacement of the end-effector measured using cable-type encoders is shown in Fig. 13.

As shown in Fig. 13, the end-effector is driven to

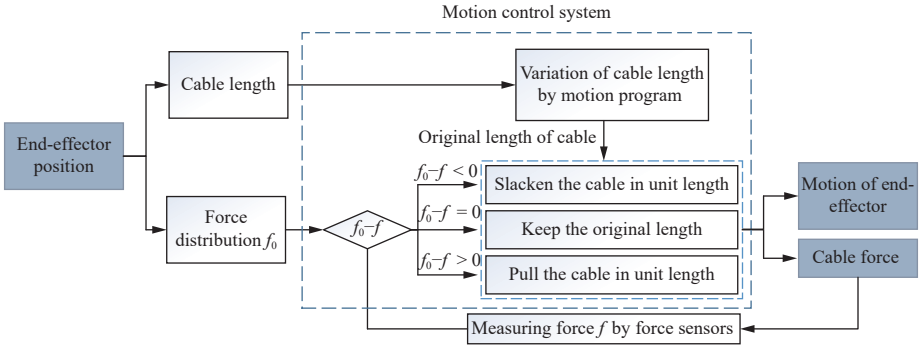

Fig. 11 Force-position mix control strategy

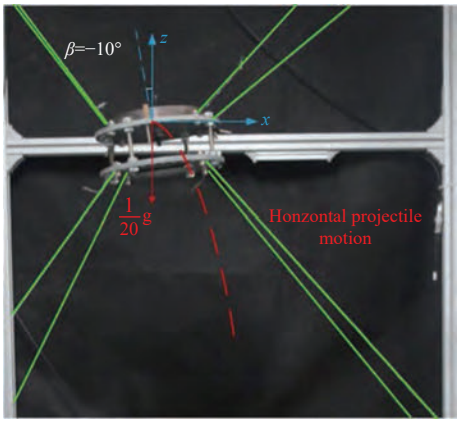

Fig. 12 Motion of low gravity simulation experiment

achieve horizontal projection under $\frac{1}{20}$ gravity. The change of actual displacement with time is consistent with the theoretical value. When taking the second order derivative of the fitting curve of vertical displacement, the vertical acceleration of the end-effector is $0.504\,\mathrm{m/s^2}$, which is very close to $\frac{1}{20}$ gravity. Therefore, the end-effector can be regarded to be in the $\frac{1}{20}$ gravity environment. In other words, the 8-cable driven parallel manipulator can successfully simulate the $\frac{1}{20}$ gravity environment. Further, the 8-cable driven parallel manipulator is redundantly actuated, which can control the pose of the end-effector to achieve 6-DOF motion. This can also be applied to a simulation experiment of landing in a low gravity environment.

5.3 Simulation experiment of end-force output in low gravity environment

Based on the simulation experiment of a low gravity environment, the 8-cable driven parallel manipulator is applied to output an end-force $\boldsymbol{F}$ in a $\frac{1}{20}$ gravity environment. As shown in Fig. 14, the magnitude of the end-force is $F = ma = 5.5\,\mathrm{kg} \times 0.2\,\mathrm{m/s^2} = 1.1\,\mathrm{N}$, and direction of $\boldsymbol{F}$ is $\beta = 10°$ between the z-axis and vertical direction in the XPZ plane. The acceleration of the end-effector is

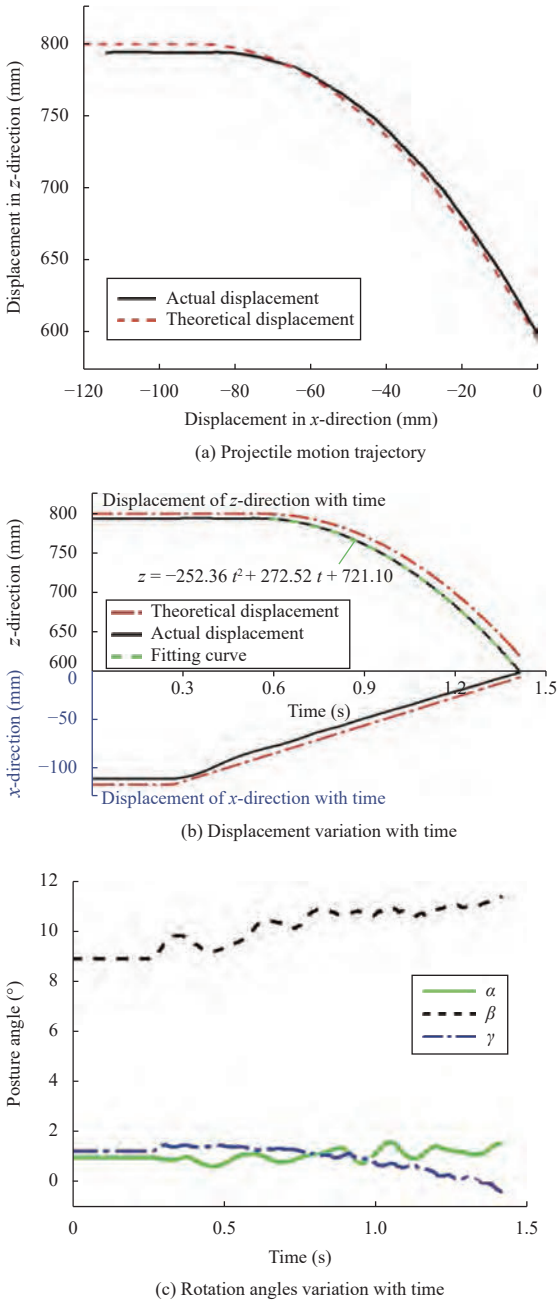

Fig. 13 Results of $\frac{1}{20}$ gravity environment simulation experiment

$a = 0.2\,\mathrm{m/s^2}$. The theoretical force distribution satisfying the above experiment design can be computed by the closed-form force distribution method. Each cable force will be controlled according to the results of force distribution with the force-position mix control strategy.

According to (8), $\boldsymbol{F}$ is a vector of cable force and the gravity of the end-effector and load, which is a force that is not directly measured by sensors. Since the gravity is a constant, the result of end-force output is equivalent to the result of the cable force. The actual unit vector $\boldsymbol{u}_i$ along the cable can be obtained by the displacement and pose of the end-effector measured by cable type encoders. The actual state of cable force control is shown in Fig. 14. The cable forces are measured by force sensors and processed by a low-pass filter. From Fig. 15, the actual results of cable force agree well with the calculated force distribution, which illustrates that the actual results of end-force output agree well with the theoretic values. This indicates that the cable force can be controlled effectively with the force-position mix control strategy. The error between the theoretical value and actual value is caused by friction loss and dimension error. The experiment result shows that the 8-cable driven parallel manipulator can be used to output the end-force in a low gravity environment.

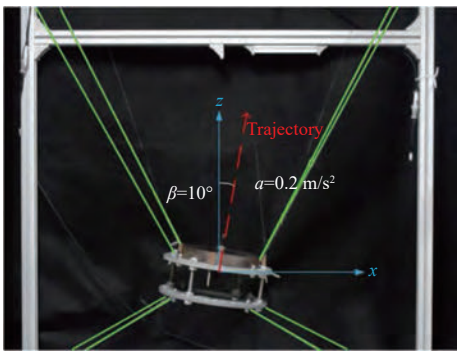

Fig. 14 Motion of low gravity simulation experiment

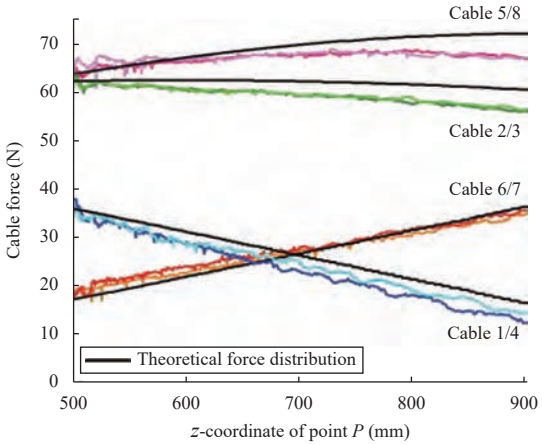

Fig. 15 Results of cable force control

6 Conclusions

In this paper, the process of end-force output and the low gravity environment simulation are studied, and the experiments are carried out using the 8-cable driven parallel manipulator. The force-position mix control strategy is applied, so that the cable force can be controlled proactively along the force distribution to realize a superposition output of the end-force and a low gravity environment. Further, the modeling of the effect of the cable force on the end-force output is presented. A study of the suitable choice for end-force output is obtained from that modeling. The experiments of end-force output and the low gravity environment simulation indicate that the cable force can be controlled effectively with the force–position mix control strategy, and the 8-cable driven parallel manipulator can be used to output end-force in a low gravity environment.

Further, the realization of cable force control is the basis for introducing the distribution acting on the end-effector, which will contribute to the dynamic characteristic research of the cable-driven mechanism, such as vibration and rigidity of the mechanism. Combining the end-force output and introduction of distribution, the simulation of a more complex situation in rocket launching will be the subject of the future work.

Acknowledgements

This research was supported by National Natural Science Foundation of China (No. 91648107), and Beijing Natural Science Foundation (No. L182041).

References

[1] F. Karmali, M. Shelhamer. The dynamics of parabolic flight: Flight characteristics and passenger percepts. *Acta Astronautica*, vol. 63, no. 5–6, pp. 594–602, 2008. DOI: 10.1016/j.actaastro.2008.04.009.

[2] Q. Y. Feng, J. F. Li, T. S. Wang. Study on weightlessness dynamics simulated by neutral buoyancy in air-driven shell. *Space Medicine & Medical Engineering*, vol. 18, no. 3, pp. 182–185, 2005. DOI: 10.3969/j.issn.1002-0837.2005.03.007. (in Chinese)

[3] L. B. Wu, X. Y. Wang, Q. Li. Fuzzy-immune PID control of a 6-DOF parallel platform for docking simulation. *Journal of Zhejiang University* (*Engineering Science*), vol. 42, no. 3, pp. 387–391, 2008. DOI: 10.3785/j.issn.1008-973X.2008.03.005. (in Chinese)

[4] H. Q. Zhang, H. R. Fang, B. S. Jiang, S. G. Wang. Dynamic performance evaluation of a redundantly actuated and over-constrained parallel manipulator. *International Journal of Automation and Computing*, vol. 16, no. 3, pp. 274–285, 2019. DOI: 10.1007/s11633-018-1147-6.

[5] Y. Sato, A. Ejiri, Y. Iida, S. Kanda, T. Maruyama, T. Uchiyama, H. Fujii. Micro-G emulation system using constant-tension suspension for a space manipulator. In *Proceedings of IEEE International Conference on Robotics and Automation*, IEEE, Sacramento, USA, pp. 1893–1900,

1991. DOI: 10.1109/ROBOT.1991.131902.

[6] G. C. White, Y. S. Xu. An active vertical-direction gravity compensation system. *IEEE Transactions on Instrumentation and Measurement*, vol. 43, no. 6, pp. 786–792, 1994. DOI: 10.1109/19.368066.

[7] R. Verhoeven. Analysis of the Workspace of Tendon-based Stewart Platforms, Ph. D. dissertation, University Duisburg-Essen, Essen, Germany, 2004.

[8] W. K. Chen. *Linear Networks and Systems*, Monterey, USA: Brooks/Cole Engineering Division, 1983.

[9] H. V. Poor. *An Introduction to Signal Detection and Estimation*, 2nd ed., New York, USA: Springer, 1994.

[10] X. Q. Tang, L. W. Tang, J. S. Wang, D. F. Sun. Workspace quality analysis and application for a completely restrained 3-Dof planar cable-driven parallel manipulator. *Journal of Mechanical Science and Technology*, vol. 27, no. 8, pp. 2391–2399, 2013. DOI: 10.1007/s12206-013-0624-7.

[11] R. Yao, X. Q. Tang, J. S. Wang, P. Huang. Dimensional optimization design of the four-cable-driven parallel manipulator in FAST. *IEEE/ASME Transactions on Mechatronics*, vol. 15, no. 6, pp. 932–941, 2010. DOI: 10.1109/TMECH.2009.2035922.

[12] X. Q. Tang, R. Yao. Dimensional design on the six-cable driven parallel manipulator of FAST. *Journal of Mechanical Design*, vol. 133, no. 11, Article number 111012, 2011. DOI: 10.1115/1.4004988.

[13] L. Nurahmi, B. Pramujati, S. Caro, Jeffrey. Dimension synthesis of suspended eight cables-driven parallel robot for search-and-rescue operation. In *Proceedings of International Conference on Advanced Mechatronics, Intelligent Manufacture, and Industrial Automation*, IEEE, Surabaya, Indonesia, pp. 237–241, 2017. DOI: 10.1109/ICAMIMIA.2017.8387594.

[14] H. Hadian, Y. Amooshahi, A. Fattah. Kinematics and dynamics modeling of a new 4-DOF cable-driven parallel manipulator. *International Journal of Intelligent Mechatronics and Robotics*, vol. 1, no. 4, pp. 44–60, 2011. DOI: 10.4018/ijimr.2011100103.

[15] A. Alamdari. Cable-driven Articulated Rehabilitation System for Gait Training, Ph. D. dissertation, State University of New York at Buffalo, USA, 2016.

[16] A. Alamdari, V. Krovi. Design and analysis of a cable-driven articulated rehabilitation system for gait training. *Journal of Mechanisms and Robotics*, vol. 8, no. 5, Article number 051018, 2016. DOI: 10.1115/1.4032274.

[17] M. Hiller, S. Q. Fang, S. Mielczarek, R. Verhoeven, D. Franitza. Design, analysis and realization of tendon-based parallel manipulators. *Mechanism and Machine Theory*, vol. 40, no. 4, pp. 429–445, 2005. DOI: 10.1016/j.mechmachtheory.2004.08.002.

[18] L. Mikelsons, T. Bruckmann, M. Hiller, D. Schramm. A real-time capable force calculation algorithm for redundant tendon-based parallel manipulators. In *Proceedings of IEEE International Conference on Robotics and Automation*, IEEE, Pasadena, USA, pp. 3869–3874, 2008. DOI: 10.1109/ROBOT.2008.4543805.

[19] X. Q. Tang, W. F. Wang, L. W. Tang. A geometrical workspace calculation method for cable-driven parallel manipulators on minimum tension condition. *Advanced Robotics*, vol. 30, no. 16, pp. 1061–1071, 2016. DOI: 10.1080/01691864.2016.1185965.

[20] C. Gosselin, M. Grenier. On the determination of the force distribution in overconstrained cable-driven parallel mechanisms. *Meccanica*, vol. 46, no. 1, pp. 3–15, 2011. DOI: 10.1007/s11012-010-9369-x.

[21] A. Pott, T. Bruckmann, L. Mikelsons. Closed-form force distribution for parallel wire robots. In *Proceedings of the 5th International Workshop on Computational Kinematics*, Springer, Berlin Heidelberg, Germany, pp. 25–34, 2009. DOI: 10.1007/978-3-642-01947-0_4.

[22] P. Henriksen. The technical writer's handbook: Writing with style and clarity. *Technical Communication*, vol. 38, no. 1, pp. 110–111, 1991.

[23] S. Chen, B. Mulgrew, P.M Grant. A clustering technique for digital communications channel equalization using radial basis function networks. *IEEE Transactions on Neural Networks*, vol. 4, no. 4, pp. 570–590, 1993. DOI: 10.1109/72.238312.

[24] A. K. Hartmann, H. Rieger. *New Optimization Algorithms in Physics*, Weinheim, Germany: Wiley-VCH, 2004.

[25] H. Lamine, S. Bennour, L. Romdhane. Design of cable-driven parallel manipulators for a specific workspace using interval analysis. *Advanced Robotics*, vol. 30, no. 9, pp. 585–594, 2016. DOI: 10.1080/01691864.2016.1142897.

[26] J. Zhang, D. Xu, Z. T. Zhang, W. S. Zhang. Position/force hybrid control system for high precision aligning of small gripper to ring object. *International Journal of Automation and Computing*, vol. 10, no. 4, pp. 360–367, 2013. DOI: 10.1007/s11633-013-0732-y.

[27] H. Q. Zhang, H. R. Fang, B. S. Jiang. Motion-force transmissibility characteristic analysis of a redundantly actuated and overconstrained parallel machine. *International Journal of Automation and Computing*, vol. 16, no. 2, pp. 150–162, 2019. DOI: 10.1007/s11633-018-1156-5.

Sen-Hao Hou received the B. Sc. degree in mechanical engineering from Beijing Institute of Technology, China in 2016. He is currently a Ph. D. dgree candidate in mechanical engineering at Tsinghua University, China.

His research interest is cable parallel robot.

E-mail: hou-sh16@mails.tsinghua.edu.cn

ORCID iD: 0000-0001-7450-9190

Xiao-Qiang Tang received the B. Sc. and M. Sc. degrees in mechanical engineering from Harbin University of Science and Technology, China in 1995 and 1998 respectively. He received the Ph. D. degree in mechanical engineering from Tsinghua University, China in 2001. He is currently a professor in Department of Mechanical Engineering, Tsinghua University, China.

His research interests include parallel manipulators, robots, and reconfigurable manufacturing technology.

E-mail: tang-xq@mail.tsinghua.edu.cn (Corresponding author)

ORCID iD: 0000-0001-8399-8416

Ling Cao received the B. Sc. and M. Sc. degrees in mechanical engineering from Tsinghua University, China in 2013 and 2016, respectively.

Her research interest is cable-driven parallel robots.

E-mail: caoling_cpa@126.com

Zhi-Wei Cui received the M. Sc. degree in mechanical engineering from Beihang University, China in 2016. He is currently a Ph. D. degree candidate in mechanical engineering at Tsinghua University, China.

His research interests include parallel manipulators and cable-driven robots.

E-mail: czw16@mails.tsinghua.edu.cn

Hai-Ning Sun received the B. Sc. degree in mechanical engineering from Shandong University, China in 2017. He is currently a Ph. D. degree candidate in mechanical engineering at Tsinghua University, China.

His research interest is cable parallel robot.

E-mail: sunhn17@mails.tsinghua.edu.cn

Ying-Wei Yan received the M. Sc. degree in mechanical engineering from Harbin University of Science and Technology, China in 1998. She is currently a senior engineer in the Postal Scientific Research and Planning Academy, China.

Her research interests include logistics system simulation and mechanism design.

E-mail: yanyingwei@163.com